Eur. Phys. J. D **28**, 101–107 (2004)
DOI: 10.1140/epjd/e2003-00290-6

THE EUROPEAN PHYSICAL JOURNAL D

Determination of electron density in a wall stabilized Ar–CO_2 thermal plasma

S. Brugeat[1] and H. Coitout[2,a]

[1] Laboratoire Arc Électrique et Plasmas Thermiques, Université Blaise Pascal, 24 avenue des Landais, 63177 Aubière Cedex, France
[2] Département Mesures Physiques, IUT d'Aubière, Université d'Auvergne, 24 avenue des Landais, 63172 Aubière Cedex, France

Received 14 April 2003 / Received in final form 5 September 2003
Published online 21 October 2003 –

Abstract. The electron density is measured in an argon-CO_2 thermal plasma by optical emission spectroscopy. Electron density is deduced from the Stark broadening of the argon line and hydrogen (H_α) line. Different theories are used and compared. The effect of CO_2 molecule upon this plasma is studied as a function of the Ar–CO_2 mixture composition and discharge current. The electron density is ranging from 3×10^{21} m^{-3} to 5.6×10^{22} m^{-3}. The influence of the arc confinement is studied and the electron density gradients are evaluated. Departure from local thermal equilibrium is also discussed.

PACS. 52.70.Kz Optical (ultraviolet, visible, infrared) measurements – 52.80.Mg Arcs; sparks; lightning; atmospheric electricity

1 Introduction

Thermal plasmas are widely applied to many applications, such as the decomposition and synthesis of material [1] and plasma spraying [2]. In several arc applications, the arc energy transfer toward the anode is used to carry out a treatment of the metallic material serving as the anode: welding, cutting [3]. The plasma parameters are not always well-known, and the calculated parameters must be checked experimentally. In these plasmas, the temperatures are not necessarily the same for all the species; a thermal or chemical disequilibrium can exist [4]. The different temperatures (electronic, excitation, vibration, rotation) and concentrations of different species (electrons, atoms, ions, molecules) can be estimated from optical emission spectroscopy measurements with appropriate assumptions. The local thermal equilibrium (LTE) assumption requires an effective exchange for energy between the electrons and the heavy particles. The establishment of LTE requires that collisions processes dominate, which implies that large electron densities must exist in the plasma. For electrons density below 10^{23} m^{-3}, substantial deviations from ionisation equilibrium (Saha equation) have to be expected. So an important parameter is the electron density which can be obtained by different methods. In time afterglow, mainly used techniques are Langmuir probes or hyper frequency resonant cavity. With Langmuir probe techniques, local values of electron density can be obtained [5,6], but it is quite difficult to measure temporal resolution of density. Moreover, Langmuir probe disturbs locally the plasma. With hyper frequency resonant cavity, only radial mean values of electron density are measured but it is easy to obtain good time resolution in the characteristic time for electron losses [7]. Electron density can also be obtained by spectroscopic measurements of the continuous background intensity which is a convenient method because it does not require a LTE state in the plasma. It has been used, in Ar plasma, for temperature less than 15000 K [8], or for arcs which electronic temperatures are higher ($T_e \cong 25000$ K) [9]. The Stark broadening of spectral lines is also used. Stark widths of transitions of singly ionised C, N, O, F and Ne have been measured in the plasma of a low pressure pulsed arc [10]. Electron density was also calculated from the Stark broadening of the H_α [11] or H_β [12,13] Balmer lines of hydrogen.

In this paper, electron densities are deduced from the Stark broadening of the Ar line and H_α line. Different theories have been compared and used: Griem [14], Hill [15], Kepple [16], Smith-Cooper-Vidal [17], Ispolatov [18] and Touma [19]. A wall-stabilised arc chamber has been built to obtain a good stability in time; which permits reproducible measurements. Electron density measurements, in an Ar–CO_2 thermal plasma at atmospheric pressure, are presented versus discharge current, and plasma composition. Two internal diameter central holes of the copper plates are used to show the influence of the arc

[a] e-mail: hubert.coitout@univ-bpclermont.fr

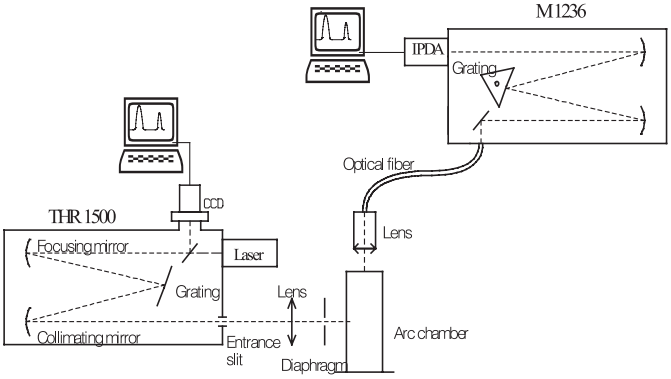

Fig. 1. Schematic diagram of the experimental setup.

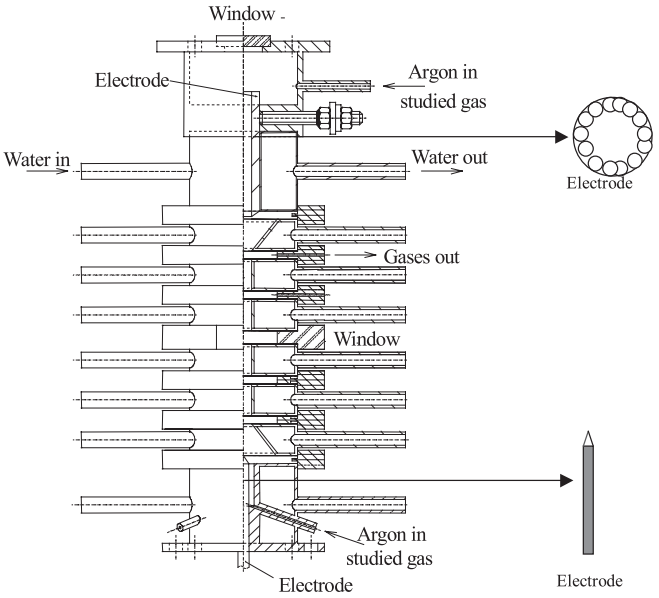

Fig. 2. Sectional view of the plasma chamber.

confinement. Electron density gradients are evaluated. Departures from LTE are also discussed.

2 Experimental device

The experimental device is shown in Figure 1. The wall stabilized arc is produced in a modified Maecker chamber which is described in detail in Figure 2. It is an 85-mm-long arc chamber, consisting of a stack of six plates of 12-mm-thick water-cooled copper plates, separated by 3-mm-thick insulating in Celoron or Bakelite spacers. The six insulating plates have 25-mm- (for the central chamber) and 35-mm-diam. central holes (for the end chambers). Concerning the copper plates, two configurations can be used: 6 or 4-mm-diam. central hole. The copper plates and insulating spacer thicknesses are very important to avoid any arc between copper plates. We require a tight chamber to avoid contamination by the surrounding air. In the center of the chamber, 5-mm-thick quartz plate plane surfaces allows the observation of the radiation emitted radially by the arc, and a disc in the top of the 20-mm-diam. chamber allows to observe in the direction of the arc axis. The quartz has an optical bandwidth from IR to UV.

The two electrodes are of tungsten with 2% thorium. The shifting of the cathodic spot is reduced on this material. On the bottom of the chamber, the electrode pin is 4 mm in diameter with a 60° taper to stabilize the spot. Eleven 3-mm-diam. tungsten rods are welded to form the hollowed electrode of the top chamber with a central hole of 6-mm-diam. This electrode allows us to obtain axial emission spectroscopic measurements.

Flow rates allow us to control the composition and velocity of the gas injected in the chamber. Two of them are used to inject the same quantity of pure argon near each electrode to protect them. The other one controls the injection of the gas studied, for example CO_2. The argon flow rate is less than 2 litres per minute and the rate of the studied gas can range from 0.5% to 10% of the total argon rate. The gas is ejected out of the chamber by four or eight holes between the center and the bottom or top of the chamber. The arc chamber is at atmospheric pressure and the airtightness is achieved by gaskets between all copper plates. The arc is initiated by moving the bottom electrode in to close proximity. After arc initiation, the electrode is returned to its initial position by the mechanism.

The arc voltage is determined by the gas mixture and current (20–60 A). For a constant intensity of 30 A, they ranged, for example, from 70 V for pure argon to 100 V for Ar–CO_2 mixtures.

The optical diagnostic experimental setup presented in Figure 1 shows two monochromators equipped with optical multichannel analyser systems which allow one to observe lines in the axis direction plasma and perpendicularly at the same time.

Concerning the radial measurements, the radiation from the arc is focused on the entrance slit of a 1.5 m Czerny-Turner monochromator. An achromatic lens is used to reduce the image of the arc by about 0.6 times and a circular diaphragm limited the effective aperture. The monochromator has an entrance slit up to 1.58 mm high and 30–80 μm wide. A laser is used to align the optical system. The chamber translation is obtained by a micrometric screw. The monochromator is equipped with a 2400 lines/mm holographic grating with a linear dispersion of about 0.2 nm/mm. A charge-coupled device (CCD) with 512×512 photo-elements of 19×19 μm each, is coupled with the monochromator. The CCD is cooled to -70 °C to reduce noise and to improve its stability.

At the top of the chamber, the radiation from the arc axis is focused on the entrance slit of a 0.5 m Czerny-Turner monochromator, the light beam of which can be translated by a micrometric screw. The monochromator has an entrance slit up to a height of 4 mm and up to a width of 25 or 75 μm. The monochromator is equipped with a 2400 lines/mm grating blazed to 500 nm with a linear dispersion of about 3 nm/mm. An intensified photodiode array, with 1024 photo-elements of 2500 μm in height$\times$25 μm in width each, is coupled with the monochromator. For each monochromator, a computer records the lines with different pause times.

All the measurement are performed at atmospheric pressure. An absolute calibration is made using a calibrated tungsten ribbon lamp.

3 Plasma diagnostic

Broadenings of spectral lines can be due, for thermal plasmas, to apparatus function, Doppler effect and Stark effect. Apparatus function and Doppler effect are Gaussian profiles. The Stark effect is reduced to a Lorentzian profile if we only take the electron broadening into account and neglect the effect of ion broadening. In the static ion approximation, the effect of ion broadening depends on the distribution of the electric microfield [20]. In this model, the motions of the perturbing plasma ions during the radiative process are ignored. On the other hand, the dynamic ion model includes the effects of ionic motions in the line shapes [21]. This effect results from the fact that the free ions of the plasma, which perturb the radiator, have enough time to move during the radiative process. Moreover, as the radiator is charged, the interactions between them and the other plasma charges are correlated to the variations of the radiator velocities [22]. These two models lead to a non analytical profile. In dense plasma, Doppler and instrumental profiles are negligible and the Stark broadening can be fitted by a Lorentzian shape [23]. In our experimental conditions, a good fit of the experimental profiles are obtained reducing the Stark effect to a Lorentzian profile. The convolution of the Gaussian and the Lorentzian profile is a Voigt profile. The electron density n_e can be determined by the Stark broadening of hydrogen and argon lines.

Due to their important broadening, hydrogen lines have been well studied to determine electron density. Griem's theory allows to calculate the broadening of few lines of the Balmer series [14]. n_e is deduced from the width at half maximum of the lines. This theory has been completed by the calculations of the broadening from the half-, quarter- and eighth width [15,16,24]. Smith, Cooper and Vidal [17] have calculated profiles of atomic lines of hydrogen (Balmer and Lyman series) for different temperatures and electron densities. The Stark broadening is calculated within the static ion approximation, neglecting the so called ion dynamic effects [25]. H_α calculated widths are reported in Table 1 for a temperature equal to 10000 K. The variations between the different calculated widths increase when n_e increases. These variations ranges, for the width at half maximum $\Delta\lambda_{1/2}$, from 0.5% ($n_e = 10^{21}$ m^{-3}) to 7.7% ($n_e = 10^{23}$ m^{-3}). For Ar thermal plasma, n_e is near 10^{22} m^{-3} [26]. For this n_e value, the variation is less than 6.5%. Different measurements [13,27–29] show that the best agreements are obtained with the unified theory of Smith, Cooper and Vidal. The half-width data of the H_α line ($\lambda = 656.26$ nm) were determined by the Smith-Cooper-Vidal theory [30]. This method, independent of local thermal equilibrium (LTE), is only requiring that the electron density distribution function be Maxwellian. As the temperature dependence is sufficiently weak, we can calculate n_e using the temperature deduced from optical emission spectroscopy measurements (absolute intensity line or Boltzmann plot). Models including ion dynamics have been developed and are based on the model microfield method [22], simulations or the frequency fluctuation model [21]. The generalized theory and the advanced general theory (AGT) of Stark broadening of hydrogen lines is again entirely semiclassical, dipole-approximation only for the impact broadening by electrons and quasistatic broadening by ions [18,23]. The effect of the acceleration of electrons by the ion field on the widths [31] and shifts [32] of spectral lines in high-density plasma has been studied using this theory. Stark full widths at half maximum of Balmer and Lyman lines have been calculated [19]. For $T = 10000$ K and n_e ranging from 10^{21} m^{-3} to 10^{23} m^{-3} the AGT overestimates the width compared to the Griem theory from 12% to 25%. Nevertheless the indirect coupling between the electron and ion broadenings (AGT) increases when n_e increases and the direct coupling between the electron and ion broadenings (AGT) increases when n_e increases and T_e decreases [23]. As the Smith, Cooper and Vidal theory underestimates the width compared to Griem theory (see Tab. 1), the uncertainty caused by the used of Smith, Cooper and Vidal theory compared with AGT is less than 15%. In our case, measurements have been performed on the H_α line which is observed without hydrogen injection in the plasma chamber. The H_β line cannot be used in Ar–CO_2 mixture due to overlapping with other lines. We also use Ar I line ($\lambda = 430.01$ nm) to determine electron density. Griem [14] has proposed a formula between width at half maximum, electron density and temperature:

$$\Delta\lambda_{1/2} = \omega(2n_e 10^{-22} + \alpha(1.11 n_e^{5/4} 10^{-27} - 7.46 n_e^{17/12} T^{-1/2} 10^{-30}))$$

where ω, α are broadening parameters (in nm) of the line by electrons and ions; T the temperature (in K) and n_e the electron density (in m^{-3}).

Chernichowski et al. [28] have also studied this line in wall stabilized Maecker chamber pure argon plasma.

Table 1. Stark widths of H_α line calculated by different theories, $T = 10000$ K.

n_e (cm^{-3})		Broadening (nm)		
		Griem theory	Kepple theory	Smith theory
10^{15}	$\Delta\lambda_{1/2}$	0.198	0.200	0.201
	$\Delta\lambda_{1/4}$	0.292	0.295	0.290
	$\Delta\lambda_{1/8}$	0.400	0.405	0.0395
10^{16}	$\Delta\lambda_{1/2}$	0.972	0.975	0.917
	$\Delta\lambda_{1/4}$	1.470	1.480	1.330
	$\Delta\lambda_{1/8}$	2.070	2.060	1.870
10^{17}	$\Delta\lambda_{1/2}$	4.830	4.590	4.260
	$\Delta\lambda_{1/4}$	7.540	7.000	6.300
	$\Delta\lambda_{1/8}$	10.80	10.00	8.940

They have proposed the following relation:

$$\ln(n_e) = 60.332 + 0.992\ln(\Delta\lambda_{1/2}) - 0.612\ln(T).$$

The recorded profiles are assumed to be Voigt profiles because they are the convolution of Gaussian profiles (Doppler broadening, apparatus function) and Lorentzian profiles (Stark broadening). First we calculated the Voigt profile which best fitted the experimental profile. The Voigt width at half maximum $\Delta\lambda_V$ is determined. We calculate the Lorentzian width at half maximum $\Delta\lambda_L$ from the formula proposed by Becker-De Mos [33] based on Allen's calculations [34]:

$$\Delta\lambda_L = \frac{(\Delta\lambda_V)^2 - (\Delta\lambda_G)^2}{\Delta\lambda_V}$$

where $\Delta\lambda_G$ is the Gaussian width at half maximum given by:

$$(\Delta\lambda_G)^2 = (\Delta\lambda_D)^2 + (\Delta\lambda_A)^2$$

$\Delta\lambda_A$ is the apparatus function width at half maximum. The value is deduced from the measurement of an atomic mercury line produced by a spectral lamp.

$\Delta\lambda_D$ is the Doppler width at half maximum. The value (in Å) is calculated:

$$\Delta\lambda_D = 7.16 \times 10^{-7}\lambda_0\sqrt{\frac{T}{M}}$$

where M is the mass in g, λ_0 the central wavelength in Å and T the temperature in K. T is deduced from the absolute intensity of atomic lines or Boltzmann plot from atomic lines.

The so deduced $\Delta\lambda_L$ allows to determine the electron density n_e.

In our wall stabilized plasma, the radial component of the electric field can be considered equal to zero and the ambipolar component negligible. The axial component can be considered independent of the plasma axis. With these assumptions, the axial electric field can be deduced from the measurement of the potential between two points of the plasma column. Probes can be used but the plasma can be disturbed by these tungsten probes. On these probes, deposits which perturb the measurements are often observed [35]. Potential falls, which are more important in the regions near electrodes, are not dependent of the arc length. Then the axial electric field is obtained by the voltage measurements between the two electrodes, for different inter-electrodes lengths of the plasma chamber.

4 Results

Axial and radial measurements have been performed for 4 mm and 6 mm-internal diameter. With the cylindrical symmetry of our arc discharge, the local intensity is deduced, for radial measurements using the Abel's inversion. Spline functions are used to smooth the experimental profile [36]. Measurements for different positions along the axis show that the electron density is constant for a given value of the radial coordinate r. In the axis of the column, results of axial and radial measurements are similar. All the electron density profiles described come from radial measurements.

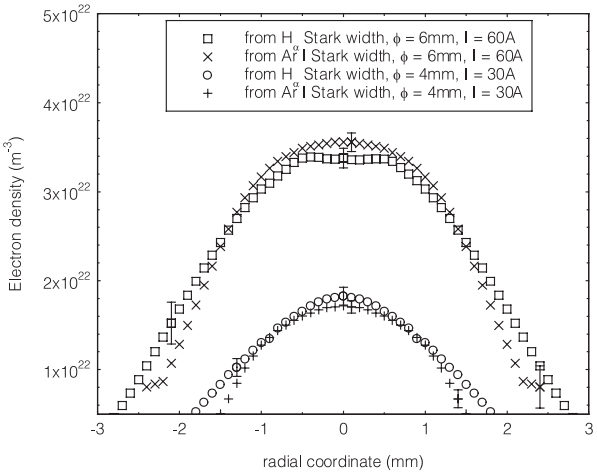

Fig. 3. Electron density profiles for two internal diameters.

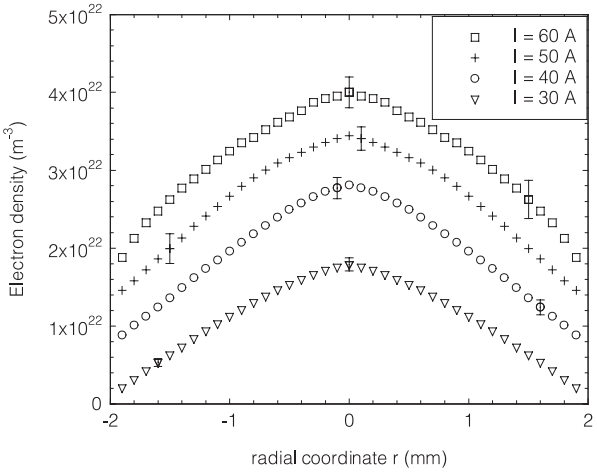

Fig. 4. Electron density profiles in a pure argon plasma; 4 mm-internal diameter.

Figure 3 presents the electron density versus the radial coordinate r for 4 mm and 6 mm-internal diameter. Whatever the discharge currents and the internal diameters are, the values of the electron density obtained by the Stark's width of H_α or Ar I ($\lambda = 430.01$ nm) lines are similar. Due to overlapping of the Ar I ($\lambda = 430.01$ nm) in Ar–CO_2 mixtures, the Stark width of H_α line has been next used.

4.1 Pure argon

Figure 4 shows electron density profiles for different discharge currents. Electron density ranges from 1.8×10^{22} m^{-3} to 4×10^{22} m^{-3} on the axis of the plasma to 3×10^{21} m^{-3} to 2×10^{22} m^{-3} in the side. n_e increases with discharge current. n_e gradient exists in the sides of the column.

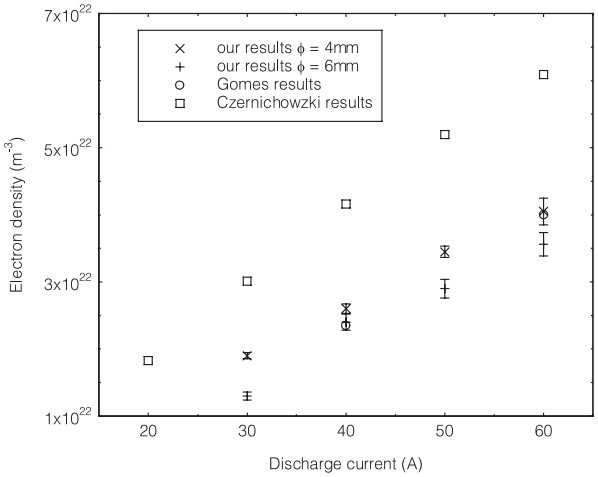

Fig. 5. Electron density versus discharge current for $r = 0$ and two internal diameters in a pure argon plasma; comparison of our results with others authors.

Figure 5 presents the electron density versus discharge current for $r = 0$ and 4 mm- and 6 mm-internal diameter. n_e for 4 mm-internal diameter is higher than n_e for 6 mm-internal diameter independently of the discharge current. When the internal diameter is smaller, plasma is more confined and plasma temperature increases, ionisation processes are more important, consequently n^+_{Ar} and n_e increase. These results are lower than results obtained by Czernichowski [28] and are in good agreement with Gomes et al. results [26], two studies carried out in a 6 mm-internal diameter wall stabilized chamber. Differences can be explained by the internal diameter in the optical measurement region. The internal diameter of the quartz cuppel is around 25 mm. Plasma is less confined in this region, plasma diameter tends to increase, temperature decreases. Ionisation processes are less effective, so n_e decreases. Although this temperature decrease is weak, it can explain the differences. The different n_e calculation methods can also explain the differences between authors.

LTE hypotheses require that temperature and densities gradients are not important. Validity tests of LTE depend on plasma. In our plasma, UV resonance line are significantly reabsorbed by the plasma, for a temperature of 10000 K, Griem [14] proposed a bottom value of n_e near 10^{22} m^{-3}. We have evaluated the relative difference between electron temperature T_e and heavy particle temperature T_h from the Chapelle's formula [37]:

$$\frac{T_e - T_h}{T_e} = 2.42 \times 10^{22} E^2 \left(\frac{k_B T_e}{E_H}\right)^2 \frac{m_e}{m_h}\frac{1}{n_e}$$

where T_e and T_h are respectively the electron temperature and heavy particle temperature in eV, E the electric field in Vm^{-1}, E_H the ionisation energy of the hydrogen atom in eV, m_e and m_h respectively the electron mass and argon atom mass in kg and n_e the electron density in m^{-3}. Axial electric field measurements are reported in Table 2. Results are similar for 4 mm- and 6 mm-internal diameter. Figure 6 shows a very weak departure from LTE

Table 2. Axial electric field in a pure argon plasma; 6 mm-internal diameter.

Intensity (A)	Electric field (V m^{-1})
30	619
40	668
50	733
60	753

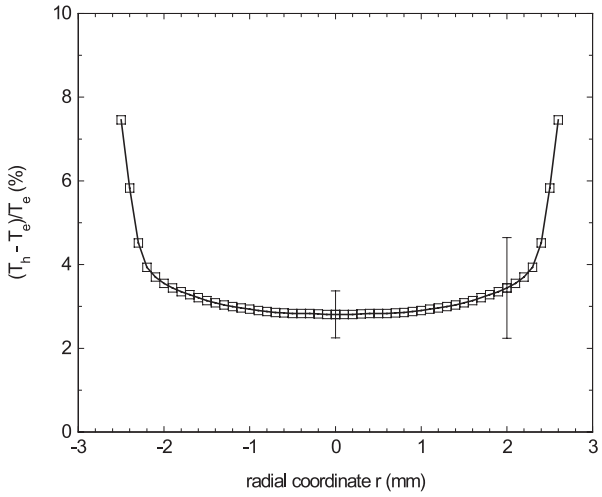

Fig. 6. Difference between electron temperature and heavy particle temperature in a pure argon plasma 6 mm-internal diameter, $I = 30$ A.

(less than 3%) on the axis of the column. These results are in good agreement with calculations of Finkelnburg and Maecker [38] and De Izarra [39]. The departure increases on the sides of the column where n_e is lower. Variation of $T_e - T_h$ has been measured in an argon transferred arc by Bouaziz et al. [40]. With a 15 A discharge current, n_e is equal to 8×10^{21} m^{-3} and $(T_e - T_h)/T_e$ ranges from 5.3% on the axis of the column ($r = 0$) to 8.6% ($r = 2.5$ mm) for a 350 V/m electric field and from 9.7% ($r = 0$) to 16% ($r = 2.5$ mm) for a 500 V/m electric field. Benilov [41] has calculated these departures for a discharge current less than 30 A. Gomez [26] has measured the departure from LTE, in pure argon plasma for $n_e < 3 \times 10^{22}$ m^{-3} and $T_e < 10700$ K.

4.2 Ar–CO_2 mixture

Figure 7 shows, in an Ar–CO_2 mixture (95% vol. Ar–5% vol. CO_2), and 4 mm- and 6mm-internal diameter, the electron densities on the axis of the plasma column. For the two internal diameters, the n_e increase is linear with the discharge current. The increase of confinement involves that n_e increases for the same reasons as in pure argon.

Figure 8 shows that n_e on the axis of the column ($r = 0$) decreases slightly when the CO_2 percentage volume increases independently of the internal diameter. The n_e values in a pure argon plasma are also reported in

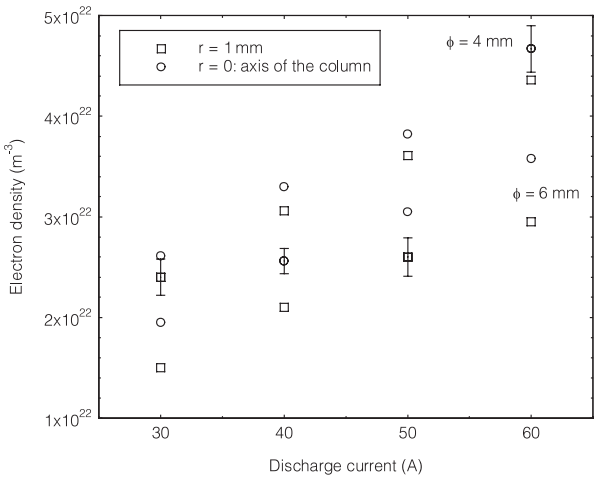

Fig. 7. Electron density versus discharge current for $r = 0$ and $r = 1$ mm and two internal diameters in a 95% vol. Ar–5% vol. CO_2 mixture.

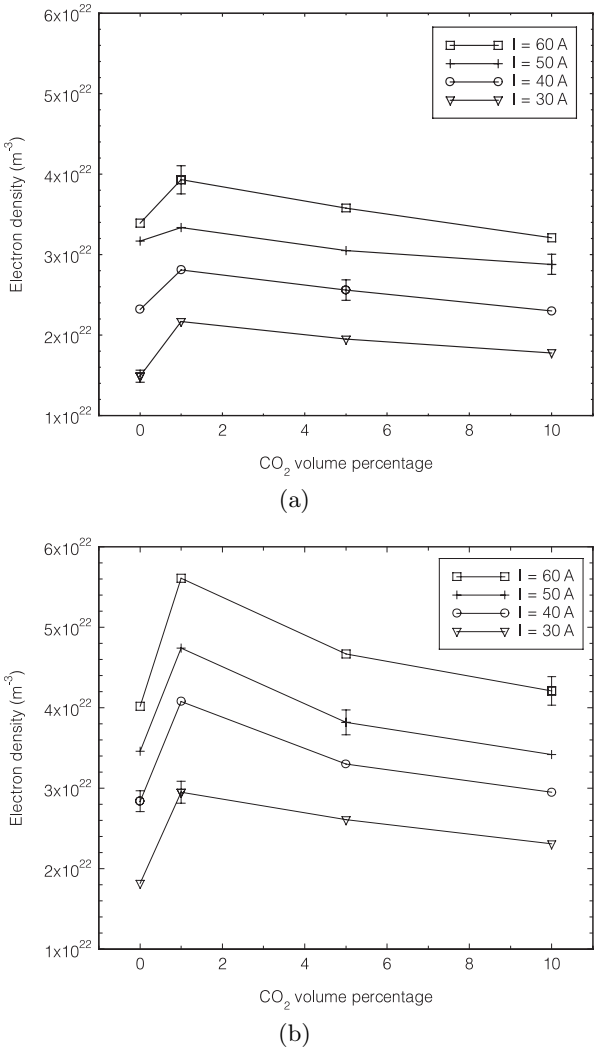

Fig. 8. Electron density versus the Ar–CO_2 mixture composition in volume percentage for $r = 0$. (a) 6 mm-internal diameter, (b) 4 mm-internal diameter.

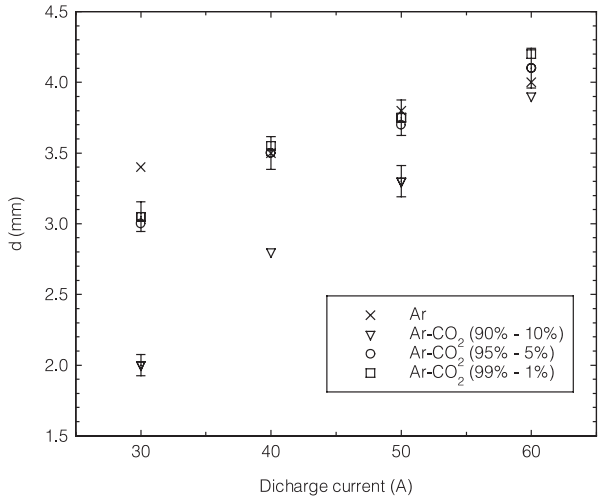

Fig. 9. Parameter d versus discharge current for different Ar–CO_2 mixture composition in volume percentage; 6 mm-internal diameter.

Figure 8. These n_e values are lower than n_e values in Ar–CO_2 mixtures even in mixtures with a weak CO_2 percentage (99.5% vol. Ar–0.5% vol. CO_2). The ionisation energies of the different atoms of the plasma can explain this phenomenon. The ionisation energies of atoms are equal to 15.5 eV for argon, 13.6 eV for oxygen and 11.2 eV for carbon. In the Ar–CO_2 mixture, the ionisation process is more efficient than in pure argon due the lower ionisation energies of carbon and oxygen, so n_e increases. Emission optical spectroscopy measurements of the Swan system of the C_2 radical have shown that the C_2 concentration is higher at the periphery of the arc column than on the axis. Carbon on the side of the discharge may increase the arc conductivity which increases the electric conduction radius. This means that current flows through a larger diameter. This factor, probably more influent than ionisation processes increases due to the lower ionisation energies of carbon and oxygen, involves that electron density decrease on the axis of the column. LTE calculations [36] predict that n_e increases when the CO_2 percentage volume increases in our range of temperature. Beuthe describes a chemical kinetic model for an Ar–CO_2 mixture based on the continuity equations and transport equations [42]. This model allows the calculations of the densities of the different species and to evaluate the main reactions in the plasma [43,44]. This model shows no evolution of n_e with the CO_2 percentage volume. Differences between these calculations and our results can be due to LTE hypothesis which is certainly true on the axis of the column but less verified in the sides of the discharge.

n_e is maximum on the axis of the column. To evaluate the n_e rate of variation, we introduce a parameter d which is the radial distance for which n_e is divided by a factor two. So, when d decreases, the rate of variation increases. Figure 9 shows that d increases when the discharge current increases independently of the plasma composition (Ar–CO_2 mixture or pure argon). This increase is weak in a pure argon plasma. It is more important in

Ar–CO_2 mixtures with a low percentage of CO_2. d increases when the CO_2 percentage volume decreases. At low current, CO_2 molecules are not completely dissociated mainly in the sides because excitation and ionisation processes which are efficient on the axis of the column are less efficient in the sides. When the current increases, these processes become efficient on the whole of the plasma, the rate of variation of n_e decreases, so d increases. This phenomenon is less important in pure argon. The plasma energy is not used to populate the very important rotational and vibrational levels of the CO_2 molecule. At low currents, in the sides of the discharge, carbon is mainly ionized because its ionisation energy is lower than Ar ionisation energy. This effect is all the more important as the CO_2 percentage is high, so d decreases when CO_2 percentage increases whatever the discharge current is. In Ar–CO_2 mixtures, metallic vapours can exist due to the erosion of electrode which is observed after many hours of use. Even if this phenomena is weak (no tungsten line is observed by optical spectroscopy), it can explain n_e variations in the electrodes regions.

Figures 5, 7 and 8 show the influence of the plasma confinement. n_e have been measured for the two configurations of the copper plates: 4- or 6-mm-diam. central hole. Whatever the plasma composition is and whatever the discharge current is, n_e is higher with the 4 mm configuration. For a given current, lower is the plasma diameter, higher is the current density so n_e.

5 Conclusion

The optical emission spectroscopy technique gives a nonperturbative and accurate electron density measurement. This method allows one to determine the electron density in an argon–CO_2 thermal plasma. The effect of CO_2 molecule upon this plasma is studied as a function of the Ar–CO_2 mixture composition and discharge current. n_e radial distributions have been deduced using Abel' inversion. n_e is ranging from 3×10^{21} m^{-3} to 5.6×10^{22} m^{-3}. The rate of variation of n_e decreases when the discharge current increases independently of the mixture composition and when the CO_2 percentage volume decreases. The influence of the arc confinement has been discussed. In pure argon plasma, a very weak (less than 3%) departure from local thermal equilibrium has been measured on the axis of the column, departure which slightly increases in the sides of the discharge.

References

1. A.C. Gentile, M.J. Kushner, J. Appl. Phys. **78**, 2074 (1995)
2. L. Gu, A.E. Arntsberg, J.A. Baken, J. High Temp. Chem. Process. **1**, 349 (1992)
3. J. Geiswiller, Meas. Sci. Technol. **9**, 1537 (1998)
4. T.L. Eddy, J. Quant. Spectrosc. Radiat. Trans. **33**, 197 (1985)
5. T. Uckan, Rev. Sci. Instrum. **58**(12), 2260 (1987)
6. E. Leveroni, E. Pfender, Rev. Sci. Instrum. **60**, 3744 (1989)
7. P. Veis, H. Coitout, L. Magne, G. Cernogora, Acta Phys. Univers. Comen. **XL**, 129 (1999)
8. S.E. Schnehage, M. Kock, E. Schulz-Gulde, J. Phys. B: At. Mol. Phys. **15**, 1131 (1982)
9. B. Pokrzywka, S. Pellerin, K. Musiol, J. Chapelle, J. Phys. D: Appl. Phys. **32**, 1665 (1999)
10. B. Blagojevic, M.V. Popovic, N. Konjevic, Phys. Scripta **59**, 374 (1999)
11. J.A. Aparicio, M.A. Gigosos, C. Perez, V.R. Gonzalez, M.I. de la Rosa, S. Mar, J. Phys. B: At. Mol. Opt. Phys. **31**, 1029 (1998)
12. N. Singh, M. Razafinimanana, A. Gleize, J. Phys. D: Appl. Phys. **31**, 2921 (1998)
13. W.L. Wiese, D.E. Kelleher, D.R. Paquette, Phys. Rev. A **6**, 1132 (1972)
14. H.R. Griem, *Plasma spectroscopy* (Mc Graw-Hill, New-York, 1964)
15. R.A. Hill, J. Quant. Spectrosc. Radiat. Trans. **7**, 401 (1967)
16. P. Kepple, H.R. Griem, Phys. Rew. **173**, 317 (1968)
17. E.W. Smith, J. Cooper, C.R. Vidal, J. Quant. Spectrosc. Radiat. Trans. **11**, 263 (1971)
18. Y. Ispolatov, E. Oks, J. Quant. Spectrosc. Radiat. Trans. **51**, 129 (1994)
19. J.E. Touma, E. Oks, S. Alexiou, A. Derevianko, J. Quant. Spectrosc. Radiat. Trans. **65**, 543 (2000)
20. C. Stehle, J. Quant. Spectrosc. Radiat. Trans. **44**, 135 (1990)
21. V. Cardenoso, M.A. Gigosos, J. Phys. B: At. Mol. Opt. Phys. **30**, 3361 (1997)
22. C. Stehle, Astron. Astrophys. **292**, 699 (1994)
23. S.A. Flih, E. Oks Y. Vitel, J. Phys. B: At. Mol. Opt. Phys. **36**, 283 (2003)
24. H.R. Griem, *Spectral line broadening by plasmas* (New-York, 1974)
25. H.R. Griem, Contrib. Plasma Phys. **40**, 46 (2000)
26. A.M. Gomes, thesis n°847, University of Toulouse, 1978
27. R.C. Preston, J. Quant. Spectrosc. Radiat. Trans. **18**, 337 (1977)
28. A. Czernichowski, J. Chapelle, Acta Phys. Polon. A **69**, 67 (1983)
29. J.L. Chotin, J.L. Lemaire, J.P. Marque, F. Rostas, J. Phys. B **11**, 371 (1978)
30. E.W. Smith, J. Cooper, C.R. Vidal, Astrophys. Suppl. Ser. **214**, 37 (1973)
31. E. Oks, J. Quant. Spectrosc. Radiat. Trans. **65**, 405 (2000)
32. E. Oks, J. Phys. B: At. Mol. Opt. Phys. **35**, 2251 (2002)
33. B. Becker-De Mos, B. Kessler, W. Seelig, Contri. Plasma Phys. **33**, 275 (1993)
34. C.W. Allen, *Astrophysical Quantities* (Athlon Press, London, 1973)
35. M. Lagreca, Ph.D. thesis, University of Toulouse, 1981
36. E. Maouhoub, H. Coitout, M.J. Parizet, IEEE Trans. Plasma Sci. **27**, 1469 (1999)
37. J. Chapelle, thesis, Paris, 1967
38. W. Finkelnburg, H. Maecker, *Electrics Arcs and Thermal Plasmas*, Handbook of Physics **22**, 254 (1950)
39. De Izarra, Ph.D. thesis, University of Orléans, 1988
40. M. Bouaziz, A. Gleize, M. Razafinimanana, J. Appl. Phys. **84**, 4128 (1998)
41. M.S. Benilov, IEEE Trans. Plasma Sci. **27**, 5 (1999)
42. T.G. Beuthe, Master thesis, Dept. Eng. Phys., Mc Master University, Canada, 1988
43. J.S. Chang, I. Maezono, IEEE Trans. Indus. Appl. **26**, 651 (1990)
44. J.S. Chang, T.G. Beuthe, J. High Temp. Chem. Proc. **1**, 333 (1992)